Steel Mass and Meltcode Distribution in the MINOS Far Detector

David Boehnlein, Robert Hatcher, Jim Kilmer, and Jeff Nelson

October 28, 2004

Introduction

The MINOS far detector comprises 486 planes of steel, each one constructed of 8 component slabs. These are plug-welded together in two layers of four slabs each to form a roughly octagonal shape for the plane. Details of this procedure are described elsewhere.[1] The basic construction is shown in Figure 1 and Figure 2.

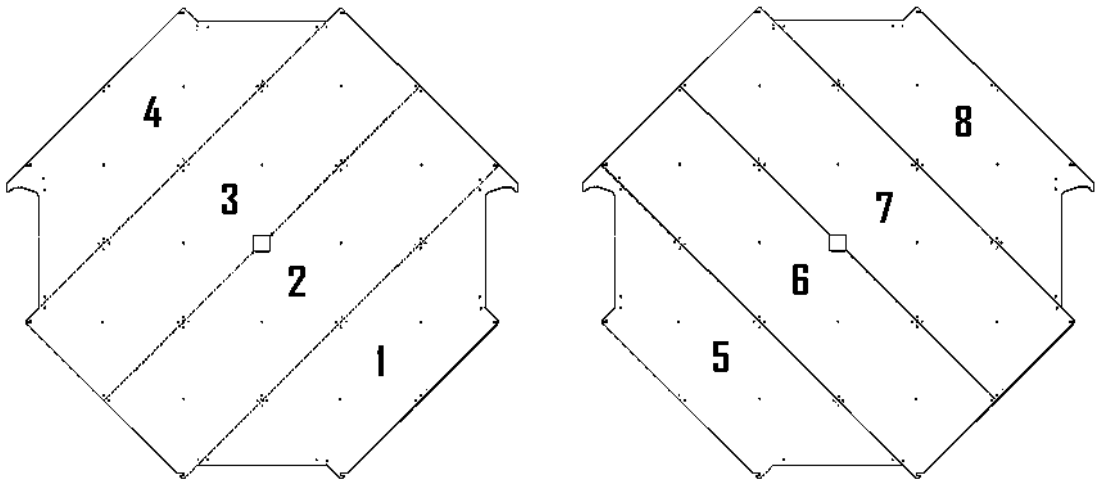

Figure 1 Arrangement of steel slabs in the two layers of a far detector plane, showing the slab numbering scheme. Part a depicts the bottom (downstream) layer; b depicts the top (upstream). The view is looking upstream. Numbering is along the u (bottom) and v (top) axes.

Each slab is identified by a part number, which specifies where it fits in the octagon; a heat number or "meltcode", which specifies the batch of steel from which it is made; and a serial number unique to that slab. As steel was delivered over the course of the far detector construction, each slab was individually weighed and the weight compared to a nominal weight for that part number. Deviations from the nominal weight are due to variations in the thickness of the steel.

[1] *MINOS Plane Assembly Procedures at the Far Detector*, NuMI Note 905 (2003).

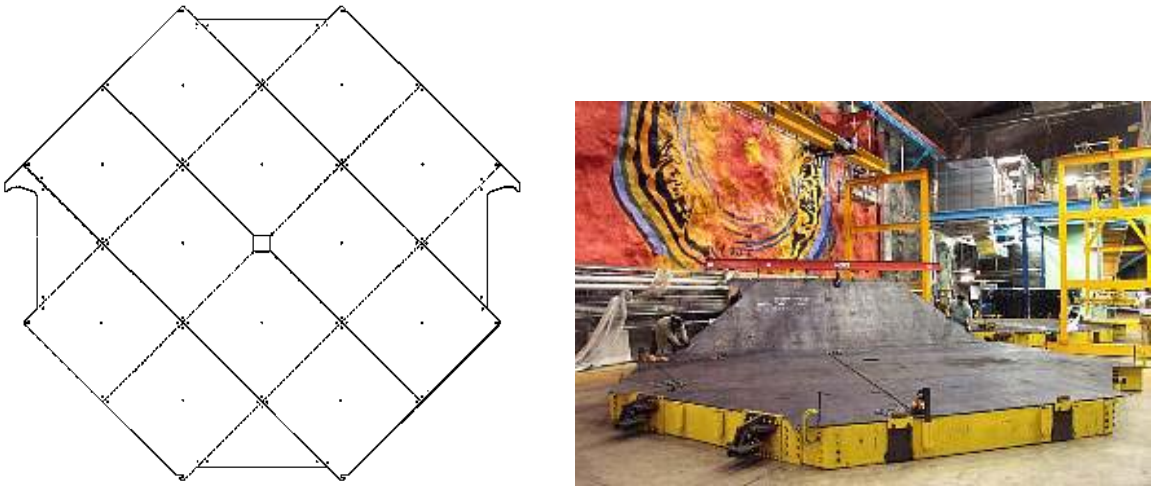

(a) (b)

Figure 2 Assembly of the far detector planes. Part a depicts the overlapping of the two-layer construction; b shows the bottom layer of a plane being assembled (photo by Jerry Meier).

This note includes three parts. The first part describes the database tables for tracking the steel slab locations and properties, the second part describes the steel mass distribution in the far detector, and the third part describes the distribution of steel heats. The importance of the heat distribution is that the chemical composition, and hence the magnetic properties, of the steel may vary from one heat to another.[2]

The Fabrication Database

The data plotted in this note are derived from two tables in the MINOS offline database: FabPlnInstall and FabSteelPlate. The FabPlnInstall table specifies the location, by plane and by position within the plane, of each steel slab and scintillator module in the MINOS far detector. The FabSteelPlate table lists the serial number, part number, heat number, nominal mass, and measured mass for each steel slab in the far detector. The Fabrication library of the MINOS offline software includes classes for working with both of these tables.

Mass Distribution of the Steel

Each of the 8 slabs that go into a MINOS steel plane is cut to a specific shape. Assuming a nominal thickness of 1.27 cm, each of the 8 part numbers has a nominal weight. The actual weight of each slab was measured with a scale in the MINOS surface building upon delivery of the steel at Soudan. The scale had a two-pound least count; all weights are converted to kilograms for this note. The scale was re-calibrated once during the far detector installation and no drifting of the response was found.[3] One may therefore assume an uncertainty of 1 kg in the slab masses and $\sqrt{8}$ kg $\approx$ 3 kg in the plane masses. The distribution of the differences between the nominal and actual weights of the slabs is shown in Figure 3. A negative value indicates that the slab is heavier than its nominal weight.

[2] *The MINOS Detectors Technical Design Report*, NuMI Note 337, p. 4-27 (1998).
[3] Jack Zorman, private communication.

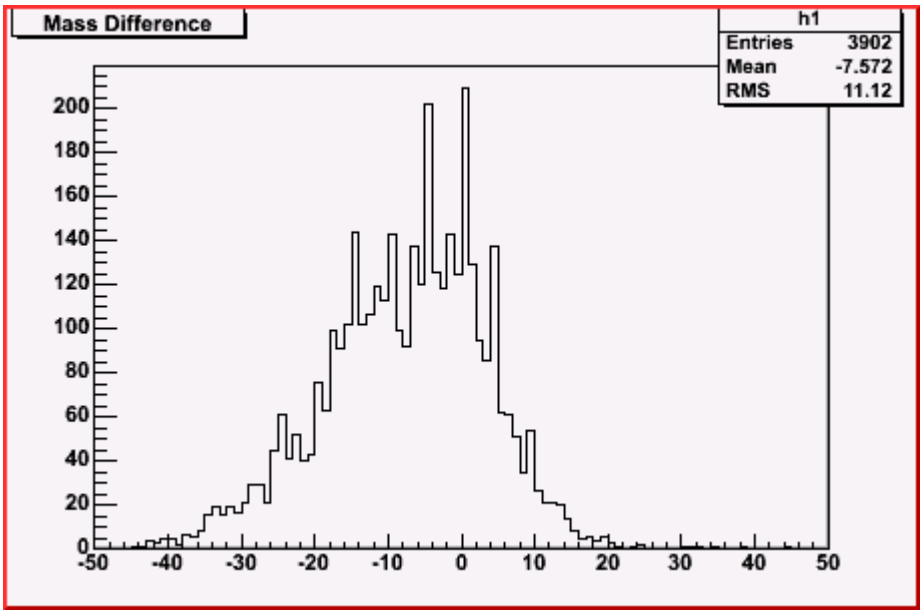

Figure 3 Mass difference (nominal – weighed) of steel slabs.

It is reasonable to assume that the mass differences are due to variations in the steel thickness from the nominal 1.27 cm. This assumption can be verified by plotting the mass differences for the inner and outer slabs separately. The inner slabs are approximately rectangular in shape, whereas the corners of the outer slabs are clipped to give the plane its octagonal shape (see Figure 1) and have roughly 75% of the area of the inner slabs. If the weight differences are due to variations in thickness, one would expect a similar ratio of the average weight differences and RMS for the outer and inner slabs. The distributions are shown in Figure 4 and Figure 5. The ratio of the average mass differences is approximately 0.73 in both cases.

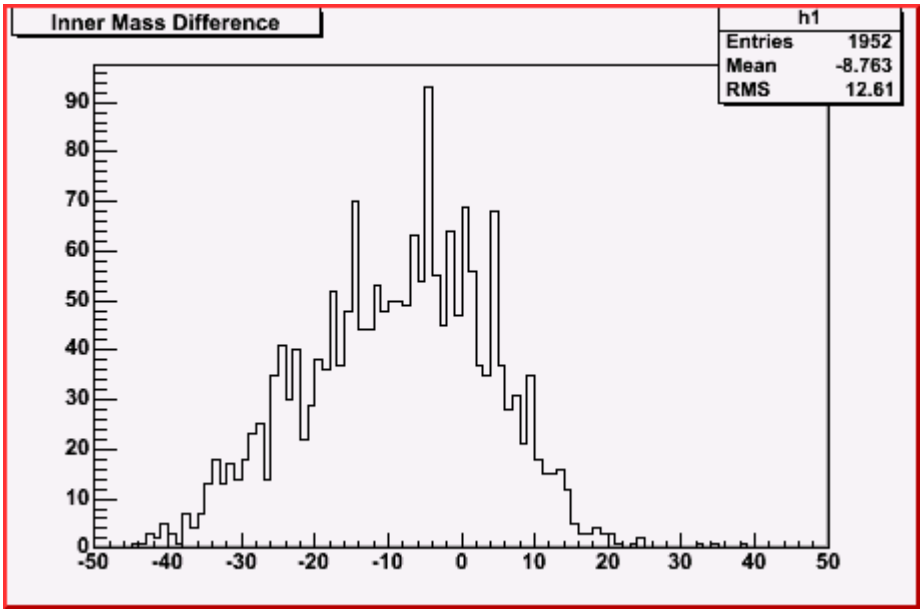

Figure 4 Mass difference (nominal – weighed) of the inner slabs.

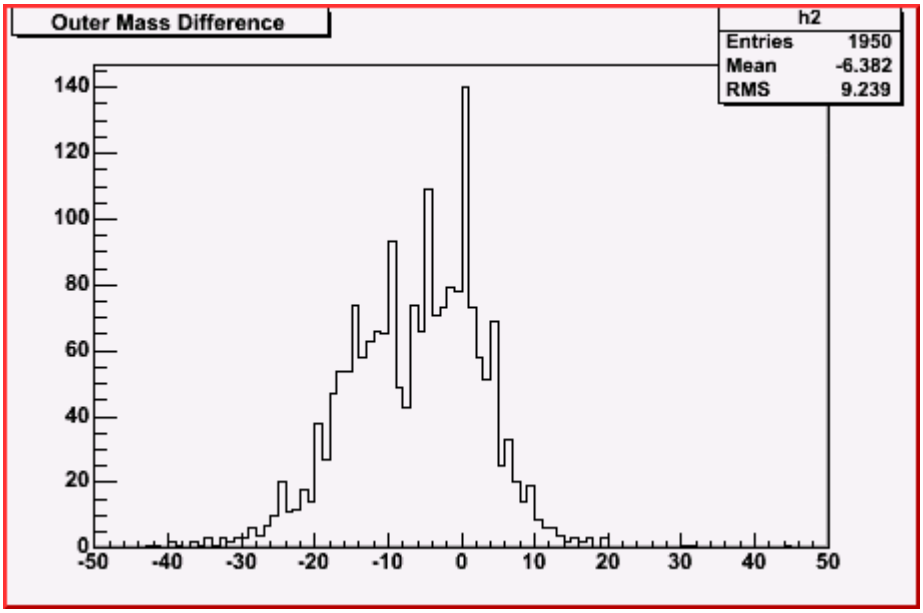

Figure 5 Mass difference (nominal – weighed) of the outer slabs.

The average difference of -7.572 kg per slab amounts to an additional 0.57% beyond the nominal steel mass of the far detector.

Figure 6 shows the mass distribution of the steel in the far detector. The sum of the 8 slab masses, in kg, is shown for each plane (Note that the vertical scale does not begin at zero.). This is simply the steel mass for each plane; the sum does not include the mass of the plug-welding material, axial bolts, collar, or scintillator modules. A plane-by-plane distribution of the mass differences is shown in Figure 7. This is the difference between the summed masses of the slabs as weighed in the surface building and the nominal plane mass. The nominal plane mass is defined here as the sum of the 8 nominal masses for the different slab types (see Table 1). Both of these figures show a mass asymmetry in the detector. The first 190 planes of the far detector are clearly heavier, on average, than the planes downstream. Average plane mass for the first 190 planes and for the planes downstream are shown in Table 1. The mass asymmetry is about 1%. Because this asymmetry reflects systematically thicker planes in the upstream part of the detector, a charged particle will lose more energy per plane in this region than it will downstream. A minimum-ionizing particle will lose about 0.3 MeV per plane more in the upstream region than in the downstream region; roughly 57 MeV for a particle passing through all 190 planes.

The uncertainty of the plane thickness can also be derived from Table 1. If one naively calculates the average mass for all of the far detector planes and divides the RMS by it, that would indicate an uncertainty of about 0.6%. However, since the upstream planes are systematically more massive than the downstream planes, it makes more sense to calculate the average and RMS for these planes separately. For the first 190 planes and

for the remainder of the detector, the uncertainty is between 0.3 - 0.4%. This is consistent with thickness measurements on near detector plates using ultrasound.[4]

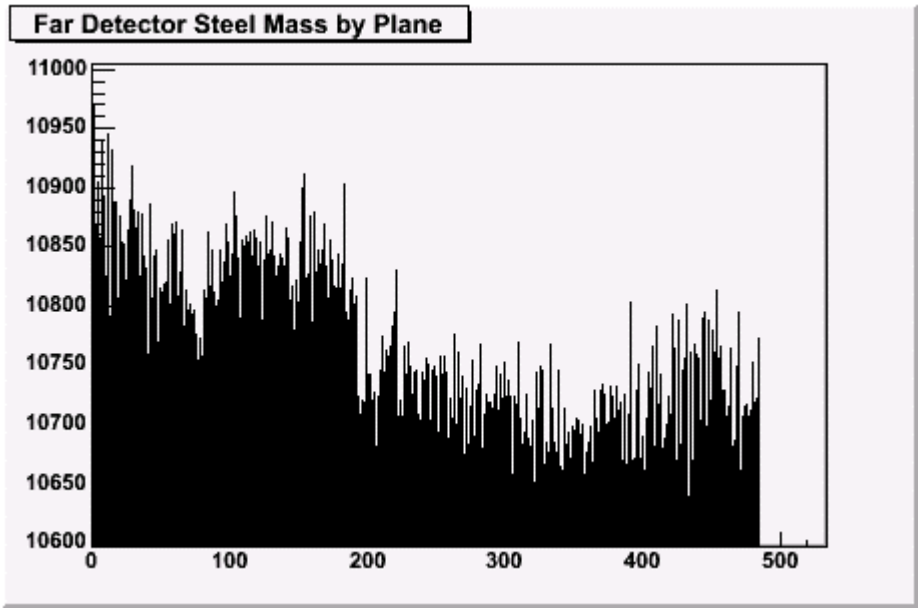

Figure 6 Plane-by-plane mass distribution of steel in the MINOS far detector.

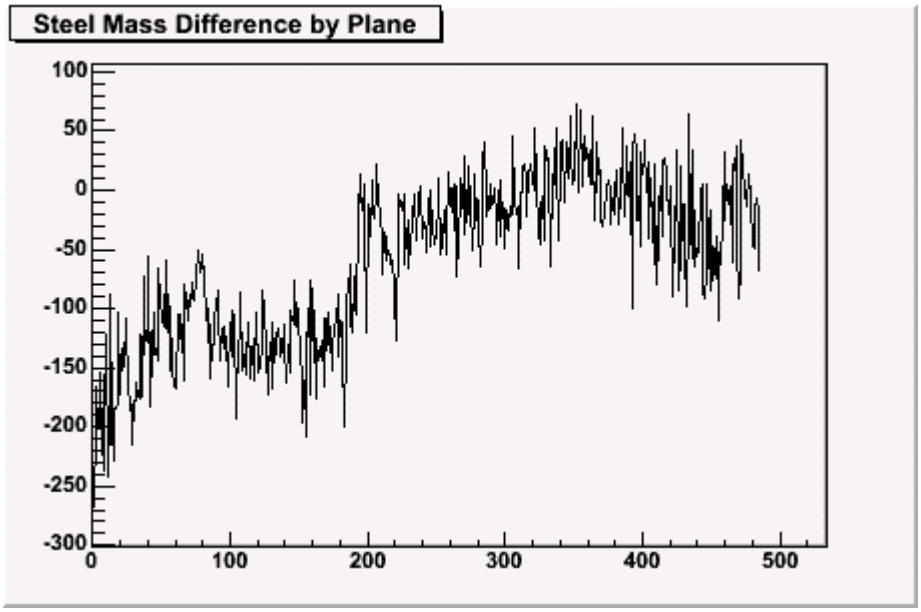

Figure 7 Plane-by-plane mass difference (nominal – weighed) distribution for steel in the MINOS far detector.

[4] Milind Diwan and Jeff Nelson, *Measurement of MINOS SteelPlates with Ultrasound,* NuMI Note 639, (2000).

	Nominal Plane	All Planes	Upstream Planes	Downstream Planes
Average Mass	10,703	10,762	10,831	10,718
RMS	n/a	67	39	37
Total Mass	5,201,861	5,230,700	2,058,000	3,172,700

Table 1 Steel data for the MINOS far detector. The nominal plane mass is the sum of the 8 nominal slab masses. Upstream planes are the first 190 planes of the detector. All masses are in kilograms.

Steel Heat Distribution

The distribution of steel heats throughout the detector is of interest, since the magnetic properties of the steel may vary from one heat to another. The number of steel heats included in any one plane may vary from one to eight. Figure 8 shows a distribution of the actual heats used per plane for the far detector. Figure 9 shows the number of heats used plane-by-plane throughout the detector. The average of 3.3 is fairly uniform throughout the detector.

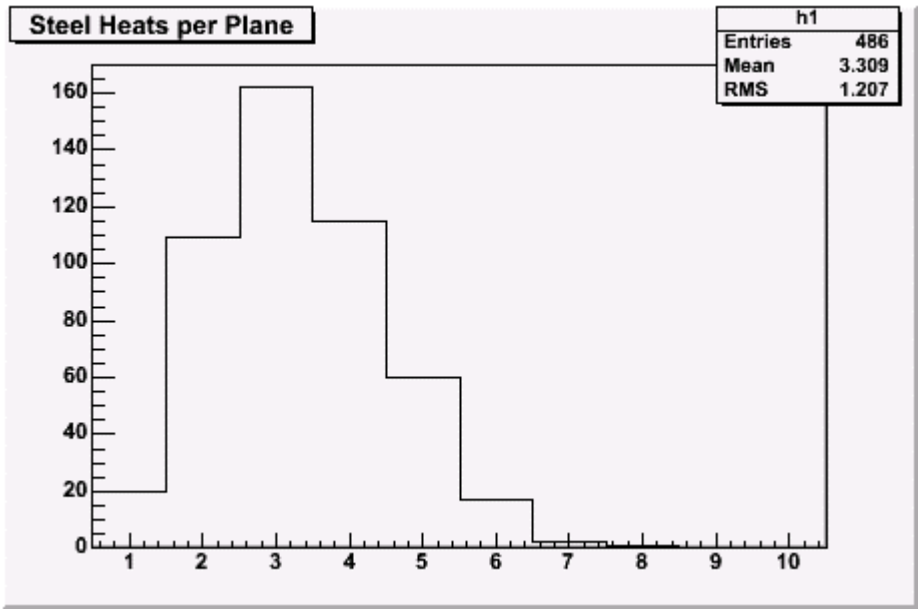

Figure 8 Number of steel heats used in construction of a single plane.

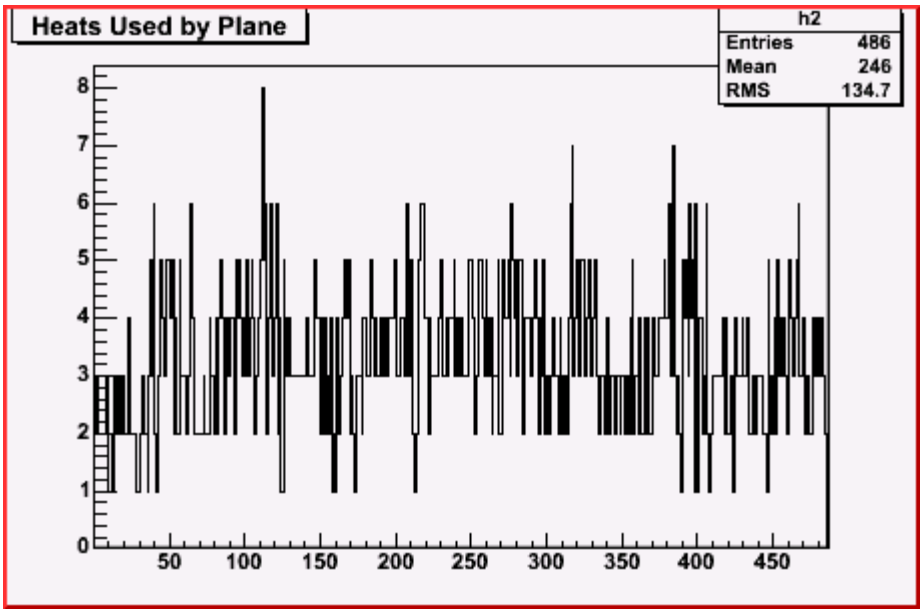

Figure 9 The number of heats per plane, shown plane-by-plane for the MINOS far detector.

The far detector slabs were produced from 45 distinct heats of steel. Figure 10 shows the distribution of the steel heats in the MINOS far detector. The vertical axis is slab position; the horizontal axis is plane number; each color corresponds to a different heat. Positions 0-3 form the "bottom", or downstream layer of steel (away from the scintillator); postions 4-7 form the "top", or upstream layer (adjacent to the scintillator).

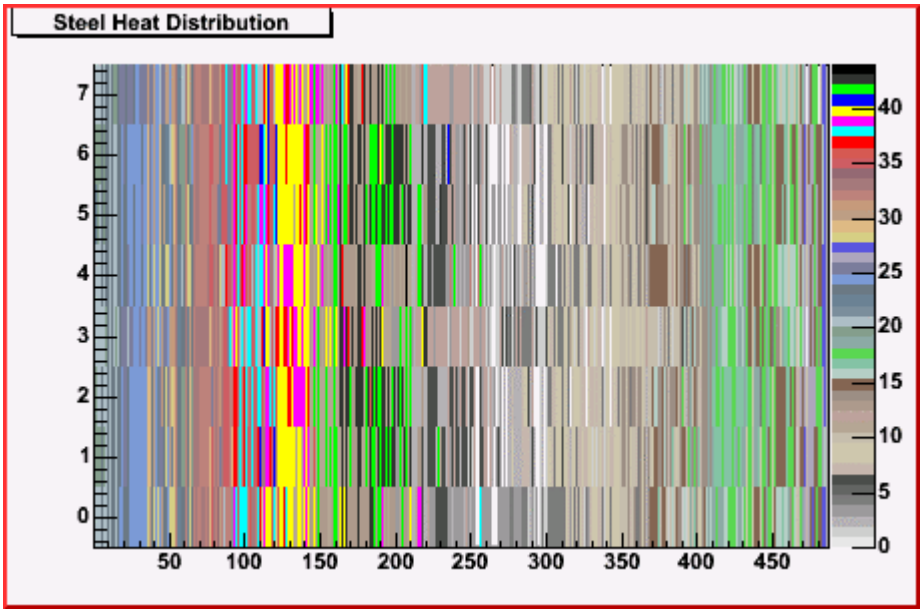

Figure 10 Heat-by-heat distribution of steel in the MINOS far detector.

A heat map showing a slab-by-slab placement of steel heats in the far detector is included as an appendix. Table 2 is a summary of how many slabs are included from each heat.

Heat #	Slabs
01640	122
02330	92
03000	149
03110	130
03220	74
03230	122
03510	57
04420	133
04600	113
04690	39
06390	129
08150	31
09410	135
10210	23
32360	59
36510	66
36530	144
37810	123
38480	128
38770	22
39170	146
39930	136
40120	18
42150	119
42160	115
43150	40
60670	3
61370	85
61680	118
63450	60
63750	144
64530	126
64830	27
66610	113
67020	118
67940	125
70300	15
70710	72
70800	133
72160	5
72370	131
72650	18
72653	2
73940	38
76270	102

Table 2 Number of slabs made from each steel heat in the far detector.

Future Work

There are several modifications and additions to the MINOS database that are natural follow-ons to the work done so far. These will allow the MINOS offline software to reconstruct events in the detector more accurately.

1. The geometry database for the MINOS detectors includes the table UgliDbiSteelPln, which describes the positions and thickness of the steel planes. At present, the table specifies the nominal 2.54 cm thickness for all of the detector planes. This table needs to be modified to include the correct steel thickness.

2. The table UgliDbiSteelPln includes a field for the meltcode, or heat number, which is presently filled with a dummy number. Putting in an actual meltcode will be problematic, since the table was concieved with the idea that each plane would comprise only a single steel heat. As Figure 8 shows, the reality is quite different. A scheme for describing a plane with a combination of heats must be implemented. One possibility is to use a 16-digit number that identifies each of the 8 slabs with one of the 45 steel heats. An alternative is to use the steel database tables directly in the field calculations and leave the meltcode column in UgliDbiSteelPln permanently dummied.

3. The heat distribution in the detector is of little use by itself. Another table describing the magnetic properties of the heats (hysteresis curves) must be developed before the heat distribution can be used to generate a more accurate field map.

4. The database must be expanded to include the steel in the near detector.

Acknowledgements

The authors are indebted to Curt Lerol and Jack Zorman at the Soudan Underground Lab for their efforts in managing the steel during the detector construction and in resolving the many post-construction questions that arose in the preparation of the database.